Chapter

The Anti-Cancer Effects of Anti-Parasite Drug Ivermectin in Ovarian Cancer

Xianquan Zhan and Na Li

Abstract

Ivermectin is an old, common, and classic anti-parasite drug, which has been found to have a broad-spectrum anti-cancer effect on multiple human cancers. This chapter will focus on the anti-cancer effects of ivermectin on ovarian cancer. First, ivermectin was found to suppress cell proliferation and growth, block cell cycle progression, and promote cell apoptosis in ovarian cancer. Second, drug pathway network, qRT-PCR, and immunoaffinity blot analyses found that ivermectin acts through molecular networks to target the key molecules in energy metabolism pathways, including PFKP in glycolysis, IDH2 and IDH3B in Kreb's cycle, ND2, ND5, CYTB, and UQCRH in oxidative phosphorylation, and MCT1 and MCT4 in lactate shuttle, to inhibit ovarian cancer growth. Third, the integrative analysis of TCGA transcriptomics and mitochondrial proteomics in ovarian cancer revealed that 16 survival-related lncRNAs were mediated by ivermectin, SILAC quantitative proteomics analysis revealed that ivermectin extensively inhibited the expressions of RNA-binding protein EIF4A3 and 116 EIF4A3-interacted genes including those key molecules in energy metabolism pathways, and also those lncRNAs regulated EIF4A3-mRNA axes. Thus, ivermectin mediated lncRNA-EIF4A3-mRNA axes in ovarian cancer to exert its anticancer capability. Further, lasso regression identified the prognostic model of ivermectin-related three-lncRNA signature (ZNRF3-AS1, SOS1-IT1, and LINC00565), which is significantly associated with overall survival and clinicopathologic characteristics in ovarian cancer patients. These ivermectin-related molecular pattern alterations benefit for prognostic assessment and personalized drug therapy toward 3P medicine practice in ovarian cancer.

Keywords: ovarian cancer, ivermectin, anti-cancer effect, therapeutic targets, prognostic assessment, biomarker, predictive preventive personalized medicine

1. Introduction

Ivermectin is chemically derived from avermectin that was discovered and isolated from soil in Jan by Omura in 1973 [1]. It was approved by Federal Drug Administration (FDA) to use for anti-parasite drug in 1987, which has significantly improved global public health as an antiparasite medicine [2]. In 2015, its discovers Drs. Omura and Campbell earned the Nobel Prize in physiology or medicine [2]. Recent years, many studies have demonstrated that ivermectin has extensive roles in anti-bacteria, anti-virus, and anticancer, except for its anti-parasite effects [3–5].

Its anticancer effect has been shown by many *in vitro* and *in vivo* experiments in multiple cancers, including ovarian cancer, breast cancer, triple-negative breast cancer, cervical cancer, lung cancer, gastric cancer, colon cancer, glioblastoma, melanoma, and leukemia [4, 6], with a wide safe and clinically reachable drug concentration of anticancer according to its pharmacokinetic range in treatment of a parasite-infected patient [7]. It offers a promising opportunity to develop a new anticancer drug via drug repositioning of this existing compound with confirmed clinical safety [8].

Ovarian cancer, a very common cancer with high mortality and poor survival in women [9, 10], are involved in multiple signaling pathway network changes [11, 12]. Many intracellular molecules and signaling pathways would be the targets of ivermectin [13]. Ivermectin have shown a potential addition role for ovarian cancer treatment. For example, ivermectin can improve the chemosensitivity of overran cancer via targeting Akt/mTOR signaling pathway [14], and can inhibit PAK1-dependent growth of ovarian cancer cells via blocking the oncogenic kinase PAK1 [15]. Ivermectin also acts as a PAK1 inhibitor to induce autophagy in breast cancer [16]. Ivermectin can enhance p53 expression and cytochrome C release, and reduce the expression levels of CDK2, CDK4, CDK6, Bcl-2, cyclin E, and cyclin D1 in glioblastoma, those promoted the cancer cell apoptosis [17]. Ivermectin can inhibit cancer cell proliferation via decreasing YAP1 protein expression in the Hippo pathway [18]. Ivermectin represses WNT-TCF pathway in WNT-TCF-dependent disease [19]. Ivermectin can promote TFE3 (Ser321) dephosphorylation to block the binding between TFE3 and 14-3-3, and induce TFE3 accumulation in the nucleus of human melanoma cells [20]. Moreover, ivermectin also affects other signaling pathway network in human cancers, including oxidative stress, mitochondrial dysfunction, angiogenesis, epithelial-mesenchymal transition, drug resistance, and stemness in tumor [6]. Thereby, ivermectin demonstrates the potential therapeutic efficiency in multiple malignant tumors.

This book chapter discussed the anti-cancer effects of ivermectin on ovarian cancer in the following aspects: (i) ivermectin inhibited cell proliferation and growth, blocked cell cycle progression, and promoted cell apoptosis in ovarian cancer [4, 21]; (ii) ivermectin inhibited ovarian cancer growth through molecular networks to target the key molecules in energy metabolism pathways, including glycolysis, Kreb's cycle, oxidative phosphorylation, and lactate shuttle pathways [21]; (iii) Integrated omics revealed that ivermectin mediated lncRNA-EIF4A3-mRNA axes in ovarian cancer to exert its anticancer capability [4, 13]; and (iv) lasso regression identified the prognostic model of ivermectin-related three-lncRNA signature (ZNRF3-AS1, SOS1-IT1, and LINC00565) that is significantly related to overall survival and clinicopathologic characteristics of ovarian cancers [4].

2. Methods

2.1 Ovarian cancer cell biological behaviors affected by ivermectin

The normal ovarian cells IOSE80 and ovarian cancer cells TOV-21 and SKOV3 were treated with ivermectin to measure ivermectin-mediated ovarian cancer cell biological behavior changes. (i) IOSE80, TOV-21G, and SKOV3 were treated with ivermectin (0–60 μM) for 24 h, followed by the use of CCK8 to measure the IC50 of ivermectin in each cell. (ii) TOV-21G and SKOV3 were treated with ivermectin (0 μM, 10 μM, 20 μM, and 30 μM) for 24 h, followed by the use of EdU assay to measure DNA synthesis in each cell. (iii) TOV-21G and SKOV3 were treated with ivermectin (0 μM, 10 μM, 20 μM, and 30 μM) for 48 h, followed by clonogenic

assay to measure the *in vitro* effects of ivermectin in each cell. (iv)TOV-21G and SKOV3 were treated with ivermectin (0 μM, 10 μM, 20 μM, and 30 μM) for 24 h, followed by flow cytometry to measure cell cycle and cell apoptosis changes in each cell. (v) When A2780 and TOV-21G seeded in 6-well plates were grown to approximately 90% confluency, followed by the use of 10-μl pipette tip to make an artificial wound, and then treated with ivermectin (0 μM, 10 μM, 20 μM, and 30 μM) for 24 h, and measure the wound healing. The relative percentage of wound healing = (the width of wound at 0 h − the width of wound at 24 h)/the width of wound at 0 h. The detailed procedure was described previously [4, 21].

2.2 Ivermectin-mediated pathway network predicted by ingenuity pathway analysis

The classical pathway network analysis software, Ingenuity Pathway Analysis (IPA) (http://www.ingenuity.com) [5] was used to predict ivermectin-related potential target molecules in three energy metabolism pathways. For this analysis, ivermectin and target genes in three energy metabolism pathways are all input into the IPA tool. The detailed procedure was described previously [21]. The predicted ivermectin-mediated targets in energy metabolism pathways were the basis for further experiment verification.

2.3 Ivermectin-mediated target molecule changes in energy metabolism pathways verified at the mRNA and protein levels

TOV-21G and SKOV3 were treated with ivermectin (0 μM, 10 μM, 20 μM, and 30 μM) for 24 h, and 48 h. At the 24 h time point, the RNAs were extracted for quantitative real-time PCR (qRT-PCR) analysis to measure the mRNA expression of target molecules (CS, PDHB, IDH2, IDH3A, IDH3B, PFKP, PKM, MCT1, MCT4, OGDHL, ND2, ND5, CYTB, and UQCRH) in energy metabolism pathways. At the 48 h time point, the proteins were extracted for Western blot analysis to measure the protein expression of target molecules (CS, PDHB, IDH2, IDH3A, IDH3B, PFKP, PKM, MCT1, MCT4, OGDHL, ND2, ND5, CYTB, and UQCRH) in energy metabolism pathways. The detailed procedure was described previously [21].

2.4 Ivermectin-mediated proteome changes in ovarian cancer identified by SILAC-based quantitative proteomics

SILAC (stable isotope labeling with amino acids in cell culture)-based quantitative proteomics was used to identified differentially expressed proteins in ovarian cancer TOV-21G treated with and without 20 μM ivermectin [13]. The identified differentially expressed proteins were used for molecular network and signaling pathway analyses to obtain ivermectin-related signaling pathway networks [13]. The detailed procedure was described previously [13].

2.5 Transcriptomics and clinical data of ovarian cancer patients extracted from TCGA database

Level 3 RNA-seq V2 transcriptomics data of 411 OC patients were extracted from The Cancer Genome Atlas (TCGA) data portal (http://cancergenome.nih.gov/) with the corresponding clinical data, including cancer status (with tumor or tumor-free), clinical stage (stages IIA, IIB, IIC, IIIA, IIIB, IIIC, and IV), neoplasm histologic grade (G1, G2, G3, G4, and GX), anatomic neoplasm subdivision (right, left, and bilateral), age at initial pathologic diagnosis (aged from 30 to 87),

lymphatic invasion (yes/no), primary therapy outcome success (complete remission/response, partial remission/response, progressive disease, and stable disease), additional radiation therapy (yes/no), survival time (days), tumor residual disease (no macroscopic disease, 1–10 mm, 11–20 mm, and > 20 mm), survival status (0 = alive, and 1 = dead), and PANCAN (Pan-Cancer Atlas). TANRIC (http://ibl.mdanderson.org/tanric/design/basic/index.html) was used for survival analysis of lncRNAs in ovarian cancer. The large-scale CLIP-Seq data with starBasev 2.0 (http://starbase.sysu.edu.cn/mirCircRNA.php) was used to predict the EIF4A3-binding mRNAs. The Kaplan–Meier method relative to the log-rank test was used for survival analysis of mRNAs in ovarian cancers. Statistical significance was set as p value <0.05. GenCLiP 3 (http://ci.smu.edu.cn/genclip3/analysis.php) was used for pathway enrichment analysis of the association of EIF4A3-binding mRNAs and patient survival rates. The detailed procedure was described previously [4].

2.6 Ivermectin-related lncRNAs verified with qRT-PCR

TRizol® Reagent (Invitrogen, CA, USA) was used to extract total RNAs of cells TOV21G and A2780 treated with different concentration of ivermectin (0 μM, 10 μM, 20 μM, and 30 μM). The extracted total RNAs was reversely transcribed into cDNAs for qRT-PCR analysis of each lncRNA expression, including KIF9-AS1, HCG15, PDCD4-AS1, ZNRF3-AS1, ZNF674-AS1, LINC00565, SOS1-IT1, WWTR1-AS1, PLCH1-AS1, LINC00517, SNHG3, STARD13-IT1, AL109767.1, HOXC-AS3, LEMD1-AS1, and LBX2-AS1. Beta-actin was set as internal control for qRT-PCR analysis. The detailed procedure was described previously [4].

2.7 LncRNA-based prognostic signature optimized with lasso regression for ovarian cancers

Lasso regression means least absolute shrinkage and selection operator regression, which was used to optimize and construct lncRNA-based prognostic signature, and the glmnet R package was used to measure the association between survival risk and lncRNA signature in ovarian cancers. Moreover, univariate and multivariate Cox regression, and Kaplan–Meier method were used to identify overall survival-related clinical characteristics described above in ovarian cancers to confirm the established lncRNA-based prognostic model. The detailed procedure was described previously [4].

2.8 Statistical significance

Benjamini–Hochberg (FDR) for multiple testing was used to correct the p values of IPA, GO, and KEGG analyses. Student's t test was used for qRT-PCR and western blot data ($p < 0.05$) with data expression of mean ± SD ($n = 3$).

3. Results and discussion

3.1 Effects of ivermectin on biological behaviors of ovarian cancers

First, CCK8 experiments were used to measure cell proliferation changes between ovarian cancer cells (SKOV3; TOV-21G) and control cells (IOSE80), treated with and without ivermectin (**Figure 1**). Each type of cells was significantly inhibited by ivermectin with a dose-dependent relationship. The IC50 (half maximal inhibitory concentration) was 29.46 μM for IOSE80 cells, 20.85 μM for SKOV3,

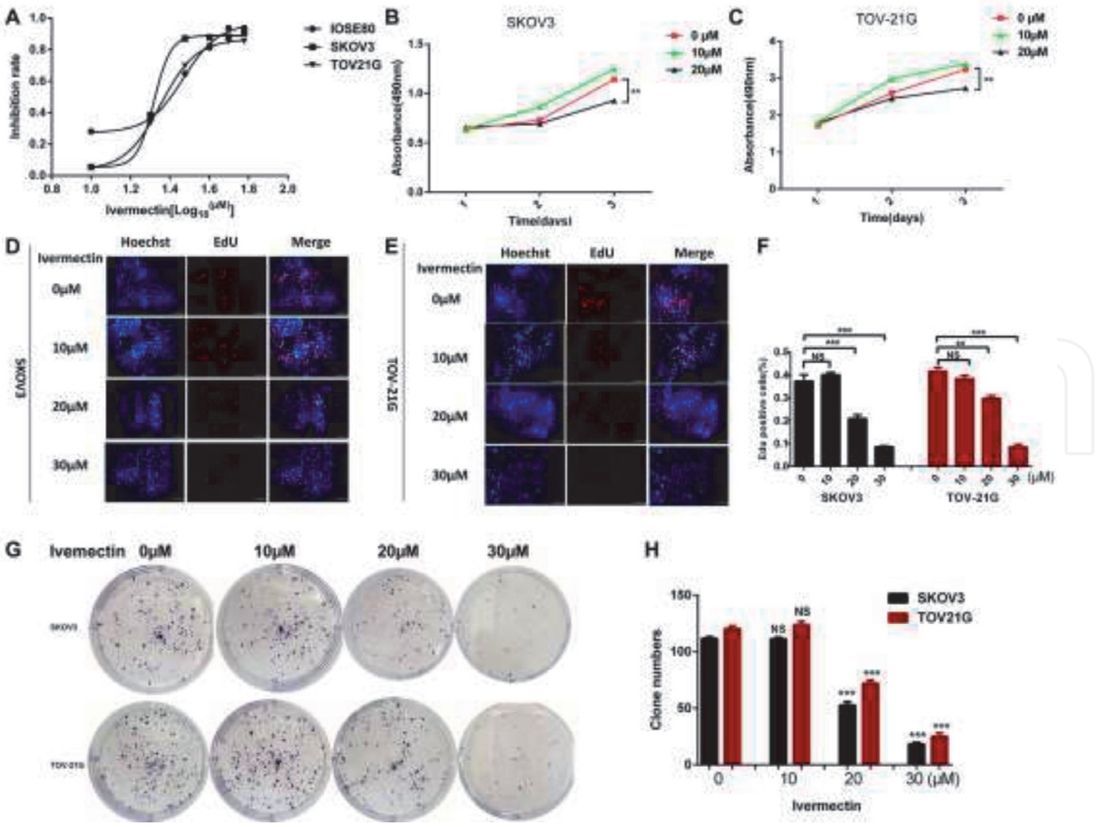

Figure 1.
Ivermectin suppressed ovarian cancer cell proliferation in vitro*, measured with CCK8 (A-C), EdU (D-F), and clonogenic experiments (G, H). Reproduced from Li et al. [21], with copyright permission from nature springer publisher, copyright 2020.*

and 22.54 μM for TOV-21G (**Figure 1A**). The IC50 of ovarian cancers were significantly lower than the normal controls. Further, 20 μM ivermectin - slightly lower than IC50 – can effectively inhibit ovarian cancer proliferation (**Figure 1B** and **C**) [21]. For *in vivo* human trial, the highest FDA-approved ivermectin dose was 200 μg/kg for human use in anti-parasite; however, a study on 68 human subjects found that the dose up to 2,000 μg/kg still worked well without CNS toxicity. The mean area under the curve ratios for the 30 and 60 mg doses were 1.24 and 1.40, indicating a minimal accumulation of ivermectin [5, 22]. These data demonstrate that ivermectin was a well-tolerated safe drug. Second, EdU cell proliferation experiments also confirmed that ivermectin significantly suppressed cell proliferation of ovarian cancers with a time-dependent relationship (**Figure 1D**-**F**) [21]. Third, Clonogenic survival experiments confirmed that ivermectin effectively inhibited the formation of cell clones with a time-dependent relationship (**Figure 1G**-**H**) [21]. Moreover, 10 μM ivermectin cannot effectively inhibit cell proliferation of ovarian cancers, 30 μM ivermectin caused cell death of ovarian cancers, and 20 μM ivermectin was a suitable dose to significantly suppress growth and proliferation of ovarian cancer cells.

3.2 Effects of ivermectin on cell cycle and apoptosis in ovarian cancers

Flow cytometry was used to measure cell cycle and apoptosis of ovarian cancer cells treated with and without ivermectin (**Figure 2**) [21]. First, the cell proportion was significantly increased in G0/G phase, decreased in S phase, and no change in G2/M phase in the high concentration (20- and 30-μM) compared to the low concentration (0- and 10-μM) of ivermectin groups (**Figure 2A**-**C**). Second, compared to control group, the proportion of apoptosis cells was significantly increased

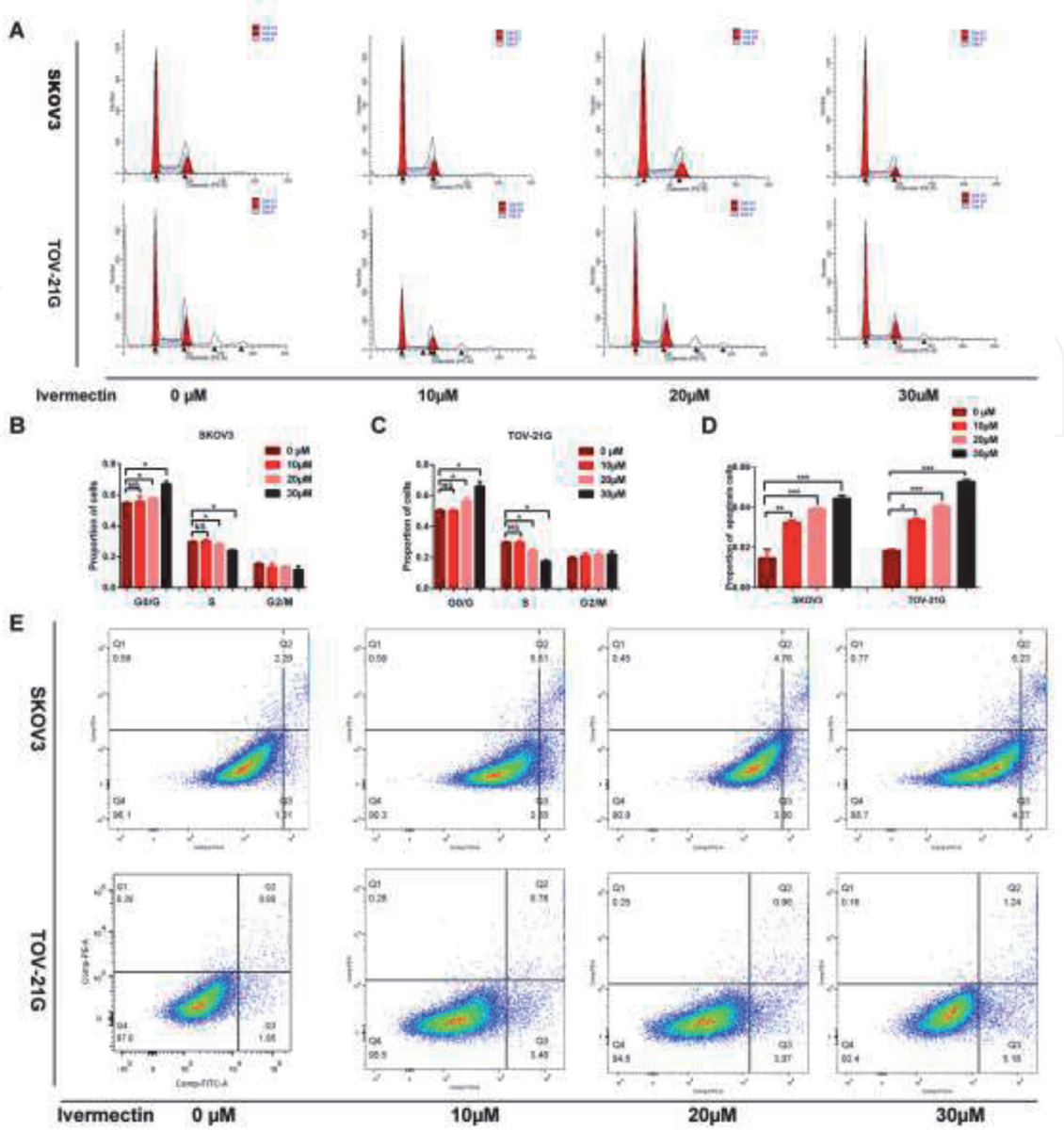

Figure 2.
Ivermectin blocked cell cycle progression (A, B, C) and promoted cell apoptosis (D, E) of ovarian cancer cells. Reproduced from Li et al. [21], with copyright permission from nature springer publisher, copyright 2020.

in different concentration of ivermectin groups, with a dose-dependent relationship (**Figure 2D** and **E**).

3.3 Effect of ivermectin on cell migration in ovarian cancers

Wound healing experiment was used to test the effect of ivermectin on cell migration of ovarian cancer cells. The results showed that cell migration was significantly inhibited in cells A2780 and TOV-21G after treatment of 20 μM and 30 μM ivermectin (**Figure 3**) [4].

3.4 Pharmaceutic molecular network predicted the association of ivermectin with ROS and energy metabolism

Ingenuity Pathway Analysis (IPA) was used for pharmaceutic molecular network analysis of ivermectin. The results showed that ivermectin was significantly

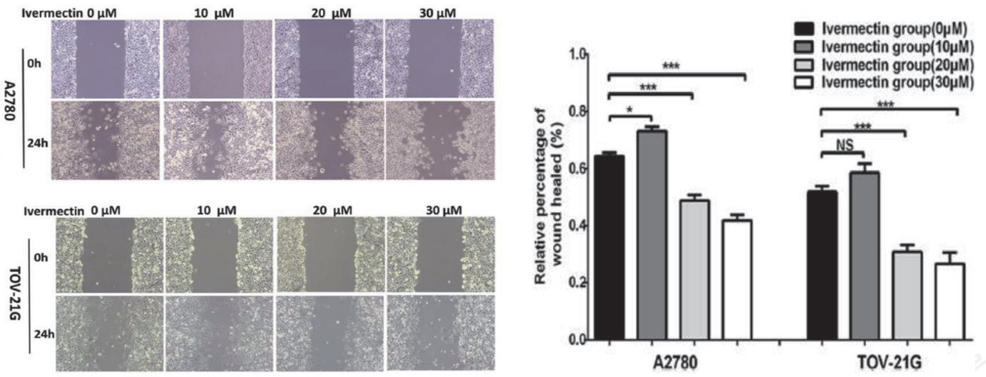

Figure 3.
Ivermectin inhibited cell migration of ovarian cancer cells TOV-21G relative to control cells A2780, analyzed with wound healing experiments. Reproduced from Li et al. [4], with copyright permission from nature springer publisher, copyright 2020.

associated with reactive oxygen species (ROS) and energy metabolism pathways, including pyruvate kinase muscle (PKM), oxoglutarate dehydrogenase L (OGDHL), mitochondrially encoded NADH dehydrogenase 2 (ND2), mitochondrially encoded NADH dehydrogenase 5 (ND5), CytB, and ubiquinolcytochrome c reductase hinge protein (UQCRH) (**Figure 4**) [21]. Moreover, ivermectin directly regulated Rbp, CYP3A4, P2RX7, ABCB1, GLRB, ABCG2, P2RX4, P glycoprotein, Abcb1b, strychnine, cytokine, and insulin; and indirectly regulated TNF, APP, MAPK1, ERK1/2, MAPK3, MAPK13, ROS, NFKBIA, testosterone, and STAT3 [21].

3.5 SILAC quantitative proteomics revealed the effects of ivermectin on key proteins in energy metabolism pathways in ovarian cancer cells

SILAC quantitative proteomics was used to detect, identify, and quantify the key protein alterations in energy metabolic pathways in ovarian cancer cells treated with (SILAC: H) and without (SILAC: L) 20 μM ivermectin for 24 h (**Table 1**) [21]. This study found that ivermectin significantly reduced (i) the expression levels of glycolysis-related enzymes, including ADH5, ENO1, GPI, GAPDH, LDHA, LDHB, PFKP, and PKM; (ii) the Kreb's cycle-related enzymes, including ACON, PCK2, PDHB, MDH2, CS, IDH2, IDH3A, IDH3B, SUCLG2, and OGDHL; (iii) the OXPHOS-related enzymes, including CYTB, UQCRH, COX17, COX1, COX6C, COX4I1, COX2, COX7A2L, COX7A2, ATP6V0C, and ATP6; and (iv) the lactate shuttle proteins MCT1 and MCT4, in ovarian cancer cells.

3.6 RT-qPCR and Western blot confirmed the effects of ivermectin on the key molecules in energy metabolism pathways at the mRNA and protein levels

RT-qPCR analysis confirmed the mRNA expression alterations of key molecules in energy metabolism pathways in ovarian cancer cells treated with ivermectin (0 μM, 10 μM, 20 μM, and 30 μM) (**Figure 5**), and further western blot analysis confirmed the protein expression alterations of those corresponding key molecules (**Figure 6**) [21]. These key molecules included PFKP, and PKM in glycolysis pathway, PDHB, CS, IDH2, IDH3A, IDH3B, and OGDHL in Kreb's cycle pathway, ND2, ND5, CYTB, and UQCRH in oxidative phosphorylation pathway, MCT1, and MCT4 in lactate shuttle. These results clearly showed that ivermectin regulated energy metabolism pathways in ovarian cancer cells.

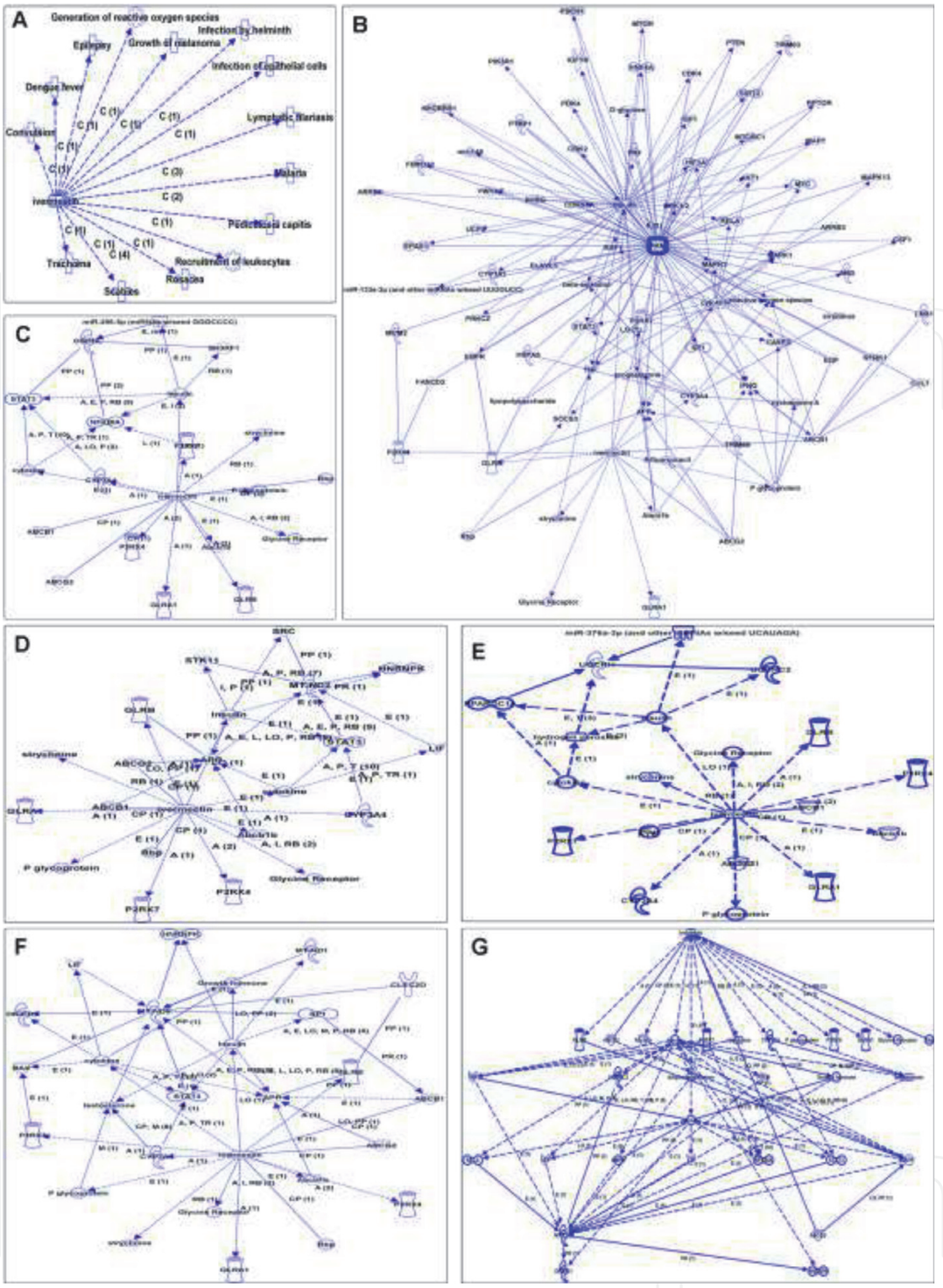

Figure 4.
Pharmaceutic molecular network predicted the associations of ivermectin with reactive oxygen species (ROS) and energy metabolism pathways (A) Disease and functional analysis of ivermectin based on IPA database (B-G). The association of ivermectin with PKM (B), OGDHL (C), ND2 (D), UQCRH (E), ND5 (F), and CYTB (G). Reproduced from Li et al. [21], with copyright permission from nature springer publisher, copyright 2020.

3.7 Ivermectin regulated lncRNA-EIF4A3-mRNA axis in ovarian cancer cells

Our quantitative mitochondrial proteomics data identified 1198 differentially mitochondrial proteins (mtDEPs) in human ovarian cancer tissues relative to control ovary tissues [11, 23]. Six RNA-binding proteins among those 1198 mtDEPs were identified, including EIF4A3, SFRS1, IGF2BP2, UPF1, C22ORF28, and EWSR1. Of them, only EIF4A3 was predicted to bind to the mRNA of key molecules in energy metabolism pathways. Further, Starbase predicted 3636 EIF4A3-biding mRNAs in various cancer; and of them, 306 EIF4A3-binding mRNAs was associated

Pathway	Protein ID	Gene name	Protein name	Q-value	Intensity H	Intensity L	Ratio H/L
Glycolysis pathway	PFKAP	PFKP	ATP-dependent 6-phosphofructokinase, platelet type	0.00E+00	14226000000	25587000000	0.54
	H3BQ34	PKM	Pyruvate kinase	7.46E-03	10727000	0	+
	ODPB	PDHB	Pyruvate dehydrogenase E1 component subunit beta, mitochondrial	0.00E+00	407280000	1649500000	0.46
	K4EN11	GAPDH	GAPDH (Fragment)	0.00E+00	0	0	/
	ENOA	ENO1	Alpha-enolase	0.00E+00	54687000000	125660000000	0.44
	F5GXY2	LDHA	L-lactate dehydrogenase A chain (Fragment)	1.00E+00	10379000	29470000	0.34
	Q5U077	LDHB	L-lactate dehydrogenase	0.00E+00	27852000000	66990000000	0.42
	A0A0A0MTS2	GPI	Glucose-6-phosphate isomerase (Fragment)	1.00E+00	56685000	138520000	0.44
	Q6IRT1	ADH5	S-(hydroxymethyl)glutathione dehydrogenase	0.00E+00	1308100000	3513700000	0.45
	B3KUV2	ACSS2	cDNA FLJ40707 fis, clone THYMU2026835, highly similar to Acetyl-coenzyme A synthetase, cytoplasmic	9.53E-03	9455200	25758000	0.73
	H3BRS6	ADPGK	ADP-dependent glucokinase (Fragment)	5.31E-04	11465000	18413000	0.69
	AL1B1	ALDH1B1	Aldehyde dehydrogenase X, mitochondrial	0.00E+00	69821000	196750000	0.45
	ALDH2	ALDH2	Aldehyde dehydrogenase, mitochondrial	0.00E+00	812240000	1822600000	0.44

Pathway	Protein ID	Gene name	Protein name	Q-value	Intensity H	Intensity L	Ratio H/L
	AL3A2	ALDH3A2	Aldehyde dehydrogenase family 3 member A2	0.00E+00	225000000	394360000	0.55
	AL9A1	ALDH9A1	4-trimethylaminobutyraldehyde dehydrogenase	0.00E+00	529020000	1322400000	0.48
	A0A024QZ64	ALDOC	Fructose-bisphosphate aldolase	0.00E+00	1104800000	2650700000	0.43
	H0YDD4	DLAT	Acetyltransferase component of pyruvate dehydrogenase complex (Fragment)	0.00E+00	530720000	1251100000	0.46
	A0A024R713	DLD	Dihydrolipoyl dehydrogenase	0.00E+00	632170000	1843800000	0.52
	Q6FHV6	ENO2	ENO2 protein	0.00E+00	618190000	2887100000	0.26
	ENOB	ENO3	Beta-enolase	0.00E+00	215810000	482340000	0.59
	B4DG62	HK1	cDNA FLJ56506, highly similar to Hexokinase-1	0.00E+00	1617000000	4075800000	0.53
	HKDC1	HKDC1	Hexokinase HKDC1	0.00E+00	132850000	568430000	0.30
	PCKGC	PCK1	Phosphoenolpyruvate carboxykinase, cytosolic [GTP]	0.00E+00	1267700	160370000	0.07
	A0A384MTT2	PCK2	Epididymis secretory sperm binding protein	0.00E+00	403190000	1032500000	0.56
	A0A024RBX9	PDHA1	Pyruvate dehydrogenase E1 component subunit alpha	0.00E+00	457490000	1353000000	0.49
	PFKAL	PFKL	ATP-dependent 6-phosphofructokinase, liver type	0.00E+00	1242500000	2567300000	0.52

Pathway	Protein ID	Gene name	Protein name	Q-value	Intensity H	Intensity L	Ratio H/L
	A0A024R0Y5	PFKM	ATP-dependent 6-phosphofructokinase	0.00E+00	1677600000	3768800000	0.47
	Q6P6D7	PGAM1	Phosphoglycerate mutase	0.00E+00	11906000000	30409000000	0.36
	A0A3B3ITK7	PGM1	Phosphoglucomutase-1	0.00E+00	721450000	1641900000	0.43
	PGM2	PGM2	Phosphoglucomutase-2	0.00E+00	144180000	423580000	0.40
	A0A024R5Z9	PKM2	Pyruvate kinase	1.00E+00	35541000	125430000	0.54
Kreb's cycle	ODPB	PDHB	Pyruvate dehydrogenase E1 component subunit beta, mitochondrial	0.00E+00	407280000	1649500000	0.46
	B4DJV2	CS	Citrate synthase	0.00E+00	2428500000	5338700000	0.45
	IDHP	IDH2	Isocitrate dehydrogenase [NADP], mitochondrial	0.00E+00	1281200000	2994300000	0.46
	IDH3A	IDH3A	Isocitrate dehydrogenase [NAD] subunit alpha, mitochondrial	0.00E+00	268600000	1119300000	0.40
	A0A087WZN1	IDH3B	Isocitrate dehydrogenase [NAD] subunit, mitochondrial	0.00E+00	142630000	477180000	0.41
	OGDHL	OGDHL	2-oxoglutarate dehydrogenase-like, mitochondrial	0.00E+00	17707000	119970000	0.56
	O75944	ACON	Aconitase (Fragment)	0.00E+00	0	48304000	—
	A0A384MTT2	PCK2	Epididymis secretory sperm binding protein	0.00E+00	403190000	1032500000	0.56

Pathway	Protein ID	Gene name	Protein name	Q-value	Intensity H	Intensity L	Ratio H/L
	Q0QF37	MDH2	Malate dehydrogenase (Fragment)	0.00E+00	5856200000	14406000000	0.42
	A0A024R325	SUCLG2	Succinate–CoA ligase [GDP-forming] subunit beta, mitochondrial	0.00E+00	232210000	779800000	0.41
	Q71UF1	ACO2	Aconitate hydratase, mitochondrial	1.00E+00	0	12950000	—
	A0A024R1Y2	ACLY	ATP-citrate synthase	0.00E+00	2033900000	4490700000	0.46
	H0YDD4	DLAT	Acetyltransferase component of pyruvate dehydrogenase complex (Fragment)	0.00E+00	530720000	1251100000	0.46
	A0A024R713	DLD	Dihydrolipoyl dehydrogenase	0.00E+00	632170000	1843800000	0.52
	Q6IBS5	DLST	DLST protein	0.00E+00	601540000	1338700000	0.53
	A0A0S2Z4C3	FH	Epididymis secretory sperm binding protein (Fragment)	0.00E+00	1498700000	3849500000	0.43
	IDH3G	IDH3G	Isocitrate dehydrogenase [NAD] subunit gamma, mitochondrial	0.00E+00	55446000	230380000	0.54
	ODO1	OGDH	2-oxoglutarate dehydrogenase, mitochondrial	0.00E+00	325090000	949610000	0.43
	A0A494C101	PC	Pyruvate carboxylase, mitochondrial (Fragment)	7.83E-04	3454600	19685000	0.28
	PCKGC	PCK1	Phosphoenolpyruvate carboxykinase, cytosolic [GTP]	0.00E+00	1267700	160370000	0.07
	A0A024RBX9	PDHA1	Pyruvate dehydrogenase E1 component subunit alpha	0.00E+00	457490000	1353000000	0.49

Pathway	Protein ID	Gene name	Protein name	Q-value	Intensity H	Intensity L	Ratio H/L
	A0A024QZ30	SDHA	Succinate dehydrogenase [ubiquinone] flavoprotein subunit, mitochondrial	0.00E+00	1096500000	2950800000	0.44
	SDHB	SDHB	Succinate dehydrogenase [ubiquinone] iron–sulfur subunit, mitochondrial	0.00E+00	143030000	516360000	0.37
	D3DVH1	SDHC	Succinate dehydrogenase complex, subunit C, integral membrane protein, 15 kDa, isoform CRAa	0.00E+00	68060000	130150000	0.46
	B7ZAF6	SUCLA2	Succinate–CoA ligase [ADP-forming] subunit beta, mitochondrial	0.00E+00	114900000	726200000	0.33
	Q6IAL5	SUCLG1	Succinate–CoA ligase [ADP/GDP-forming] subunit alpha, mitochondrial	0.00E+00	261580000	1105700000	0.34
Oxidative phosphorylation	D2Y6X2	ND5	NADH dehydrogenase subunit 5 (Fragment)	5.33E-04	4125200	24591000	0.41
	A0A1B0TCA9	CYTB	Cytochrome b (Fragment)	3.59E-03	53396000	59765000	0.55
	Q567R0	UQCRH	UQCRH protein	0.00E+00	252050000	546900000	0.51
	C9J8T6	COX17	Cytochrome c oxidase copper chaperone	0.00E+00	7643200	53020000	0.36
	Q6FGA0	COX7A2L	COX7A2L protein	5.34E-04	22802000	1280400	17.81
	U3L4G0	ATP6	ATP synthase subunit a	0.00E+00	193600000	355900000	0.73
	X2C5C9	COX1	Cytochrome c oxidase subunit 1	7.89E-04	21347000	57543000	0.38
	A0A346M047	COX2	Cytochrome c oxidase subunit II (Fragment)	0.00E+00	1046600000	2406000000	0.38

Pathway	Protein ID	Gene name	Protein name	Q-value	Intensity H	Intensity L	Ratio H/L
	H3BNI4	ATP6V0C	V-type proton ATPase proteolipid subunit	1.00E+00	11819000	33788000	0.47
	Q496I0	COX7A2	COX7A2 protein	0.00E+00	223550000	687660000	0.32
	COX6C	COX6C	Cytochrome c oxidase subunit 6C	0.00E+00	24314000	57899000	0.34
	COX41	COX4I1	Cytochrome c oxidase subunit 4 isoform 1, mitochondrial	0.00E+00	1057000000	2524600000	0.40
	AT12A	ATP12A	Potassium-transporting ATPase alpha chain 2	1.00E+00	25608000	48153000	0.50
	ATPG	ATP5F1C	ATP synthase subunit gamma, mitochondrial	0.00E+00	610730000	1752800000	0.61
	ATPD	ATP5F1D	ATP synthase subunit delta, mitochondrial	0.00E+00	173290000	378660000	0.59
	ATP5I	ATP5ME	ATP synthase subunit e, mitochondrial	0.00E+00	139860000	416580000	0.28
	ATPK	ATP5MF	ATP synthase subunit f, mitochondrial	0.00E+00	146600000	369660000	0.57
	E9PN17	ATP5MG	ATP synthase subunit g, mitochondrial	0.00E+00	501810000	1039800000	0.45
	Q5QNZ2	ATP5PB	ATP synthase F(0) complex subunit B1, mitochondrial	0.00E+00	1074900000	2486300000	0.46
	ATP5H	ATP5PD	ATP synthase subunit d, mitochondrial	0.00E+00	525070000	965510000	0.39
	ATPO	ATP5PO	ATP synthase subunit O, mitochondrial	0.00E+00	1495600000	3024300000	0.56

Pathway	Protein ID	Gene name	Protein name	Q-value	Intensity H	Intensity L	Ratio H/L
	VPP1	ATP6V0A1	V-type proton ATPase 116 kDa subunit a isoform 1	0.00E+00	98038000	557300000	0.35
	R4GN72	ATP6V0D1	V-type proton ATPase subunit d 1	0.00E+00	258530000	806720000	0.31
	VATA	ATP6V1A	V-type proton ATPase catalytic subunit A	0.00E+00	1191800000	3218800000	0.37
	VATB2	ATP6V1B2	V-type proton ATPase subunit B, brain isoform	0.00E+00	583390000	2310600000	0.35
	A0A024R9I0	ATP6V1C1	V-type proton ATPase subunit C	0.00E+00	105790000	524300000	0.36
	Q53Y06	ATP6V1E1	ATPase, H+ transporting, lysosomal 31 kDa, V1 subunit E isoform 1	0.00E+00	226190000	457540000	0.46
	A4D1K0	ATP6V1F	V-type proton ATPase subunit F	0.00E+00	72747000	287010000	0.62
	A0A024R883	ATP6V1G1	V-type proton ATPase subunit G	0.00E+00	121660000	150890000	0.58
	A0A024R7X3	ATP6V1H	V-type proton ATPase subunit H	0.00E+00	33783000	166330000	0.37
	COX15	COX15	Cytochrome c oxidase assembly protein COX15 homolog	0.00E+00	52507000	160350000	0.47
	A0A343FH12	COX3	Cytochrome c oxidase subunit 3	0.00E+00	251800000	620670000	0.40
	H3BNX8	COX5A	Cytochrome c oxidase subunit 5A, mitochondrial	0.00E+00	489640000	1451700000	0.67
	COX5B	COX5B	Cytochrome c oxidase subunit 5B, mitochondrial	0.00E+00	237370000	754990000	0.33

Pathway	Protein ID	Gene name	Protein name	Q-value	Intensity H	Intensity L	Ratio H/L
	CX6B1	COX6B1	Cytochrome c oxidase subunit 6B1	0.00E+00	278190000	1028600000	0.28
	CY1	CYC1	Cytochrome c1, heme protein, mitochondrial	0.00E+00	426190000	876770000	0.51
	Q5T1Z0	LHPP	Phospholysine phosphohistidine inorganic pyrophosphate phosphatase	9.74E-03	0	20832000	—
	D8VCQ0	ND4	NADH–ubiquinone oxidoreductase chain 4 (Fragment)	3.36E-03	3604800	7493900	0.44
	Q7Z518	NDUFA10	NADH dehydrogenase [ubiquinone] 1 alpha subcomplex subunit 10, mitochondrial	0.00E+00	46879000	194320000	0.31
	NDUAD	NDUFA13	NADH dehydrogenase [ubiquinone] 1 alpha subcomplex subunit 13	0.00E+00	43461000	261780000	0.34
	NDUA2	NDUFA2	NADH dehydrogenase [ubiquinone] 1 alpha subcomplex subunit 2	0.00E+00	35677000	165030000	0.24
	NDUA4	NDUFA4	Cytochrome c oxidase subunit NDUFA4	0.00E+00	99542000	1041400000	0.28
	NDUA5	NDUFA5	NADH dehydrogenase [ubiquinone] 1 alpha subcomplex subunit 5	0.00E+00	126370000	440540000	0.46
	NDUA8	NDUFA8	NADH dehydrogenase [ubiquinone] 1 alpha subcomplex subunit 8	0.00E+00	75771000	226560000	0.33
	NDUA9	NDUFA9	NADH dehydrogenase [ubiquinone] 1 alpha subcomplex subunit 9, mitochondrial	0.00E+00	38134000	212250000	0.38
	H3BNK3	NDUFAB1	Acyl carrier protein (Fragment)	0.00E+00	91383000	220140000	0.41
	NDUB1	NDUFB1	NADH dehydrogenase [ubiquinone] 1 beta subcomplex subunit 1	0.00E+00	52572000	104780000	0.46

Pathway	Protein ID	Gene name	Protein name	Q-value	Intensity H	Intensity L	Ratio H/L
	H3BPJ9	NDUFB10	NADH dehydrogenase [ubiquinone] 1 beta subcomplex subunit 10	0.00E+00	68400000	353550000	0.41
	NDUBB	NDUFB11	NADH dehydrogenase [ubiquinone] 1 beta subcomplex subunit 11, mitochondrial	0.00E+00	40408000	192110000	0.31
	C9JKQ2	NDUFB3	NADH dehydrogenase [ubiquinone] 1 beta subcomplex subunit 3 (Fragment)	7.84E-04	19660000	91217000	0.33
	NDUB4	NDUFB4	NADH dehydrogenase [ubiquinone] 1 beta subcomplex subunit 4	0.00E+00	15764000	129660000	0.40
	NDUB8	NDUFB8	NADH dehydrogenase [ubiquinone] 1 beta subcomplex subunit 8, mitochondrial	0.00E+00	38897000	134110000	0.34
	A0A3B3IT57	NDUFB9	NADH dehydrogenase [ubiquinone] 1 beta subcomplex subunit 9	0.00E+00	47909000	178250000	0.26
	E5KRK5	NDUFS1	Mitochondrial NADH–ubiquinone oxidoreductase 75 kDa subunit	0.00E+00	87635000	1424000000	0.27
	NDUS2	NDUFS2	NADH dehydrogenase [ubiquinone] iron–sulfur protein 2, mitochondrial	0.00E+00	255210000	555800000	0.40
	NDUS3	NDUFS3	NADH dehydrogenase [ubiquinone] iron–sulfur protein 3, mitochondrial	0.00E+00	303550000	1007100000	0.38
	H0Y9M8	NDUFS4	NADH dehydrogenase [ubiquinone] iron–sulfur protein 4, mitochondrial (Fragment)	0.00E+00	22776000	124620000	0.20
	Q6IBA0	NDUFS5	NADH dehydrogenase (Ubiquinone) Fe-S protein 5, 15 kDa (NADH-coenzyme Q reductase)	0.00E+00	13539000	83631000	0.36
	B7Z4P1	NDUFS7	cDNA FLJ58024, highly similar to NADH–ubiquinone oxidoreductase 20 kDa subunit, mitochondrial	3.38E-03	89666000	146530000	1.06
	E9PKH6	NDUFS8	NADH dehydrogenase [ubiquinone] iron–sulfur protein 8, mitochondrial (Fragment)	0.00E+00	25384000	70988000	0.38

Pathway	Protein ID	Gene name	Protein name	Q-value	Intensity H	Intensity L	Ratio H/L
	G3V0I5	NDUFV1	NADH dehydrogenase [ubiquinone] flavoprotein 1, mitochondrial	0.00E+00	25550000	98424000	0.34
	Q9UEH5	NDUFV2	24-kDa subunit of complex I (Fragment)	0.00E+00	120810000	407130000	0.33
	IPYR2	PPA2	Inorganic pyrophosphatase 2, mitochondrial	0.00E+00	815730000	1743800000	0.42
	A0A024QZ30	SDHA	Succinate dehydrogenase [ubiquinone] flavoprotein subunit, mitochondrial	0.00E+00	1096500000	2950800000	0.44
	SDHB	SDHB	Succinate dehydrogenase [ubiquinone] iron–sulfur subunit, mitochondrial	0.00E+00	143030000	516360000	0.37
	D3DVH1	SDHC	Succinate dehydrogenase complex, subunit C, integral membrane protein, 15 kDa, isoform CRAa	0.00E+00	68060000	130150000	0.46
	A0A024R5E5	TCIRG1	V-type proton ATPase subunit a	0.00E+00	139450000	227300000	0.73
	QCR9	UQCR10	Cytochrome b-c1 complex subunit 9	0.00E+00	260330000	491890000	0.52
	QCR7	UQCRB	Cytochrome b-c1 complex subunit 7	0.00E+00	208330000	523300000	0.37
	QCR1	UQCRC1	Cytochrome b-c1 complex subunit 1, mitochondrial	0.00E+00	1326400000	3772100000	0.43
	QCR2	UQCRC2	Cytochrome b-c1 complex subunit 2, mitochondrial	0.00E+00	1718400000	3636100000	0.43
	A0A384NPX8	UQCRFS1	Cytochrome b-c1 complex subunit Rieske, mitochondrial	0.00E+00	79904000	211540000	0.34
	QCR8	UQCRQ	Cytochrome b-c1 complex subunit 8	0.00E+00	88536000	237890000	0.57

Pathway	Protein ID	Gene name	Protein name	Q-value	Intensity H	Intensity L	Ratio H/L
Lactate shuttle	B4E106	MCT1	cDNA FLJ53399, highly similar to Monocarboxylate transporter 1	0.00E+00	23799000	115420000	0.53
	MOT4	MCT4	Monocarboxylate transporter 4	0.00E+00	818320000	2103700000	0.38

Table 1.
SILAC quantitative proteomics revealed the protein expression changes of key molecules in energy metabolic pathways in ovarian cancer cells TOV-21G treated with (SILAC: H) and without (SILAC: L) 20 μM ivermectin for 24 h. - means the protein expressed in L group but not in H group. + means the protein expressed in H group but not in L group. /means the protein with expressed value 0 in both H and L groups. Ratio H/L means the ratio of the ivermectin-treated group (SILAC: H) to the no ivermectin-treated group (SILAC: L). Reproduced from Li et al. [21], with copyright permission from nature springer publisher, copyright 2020.

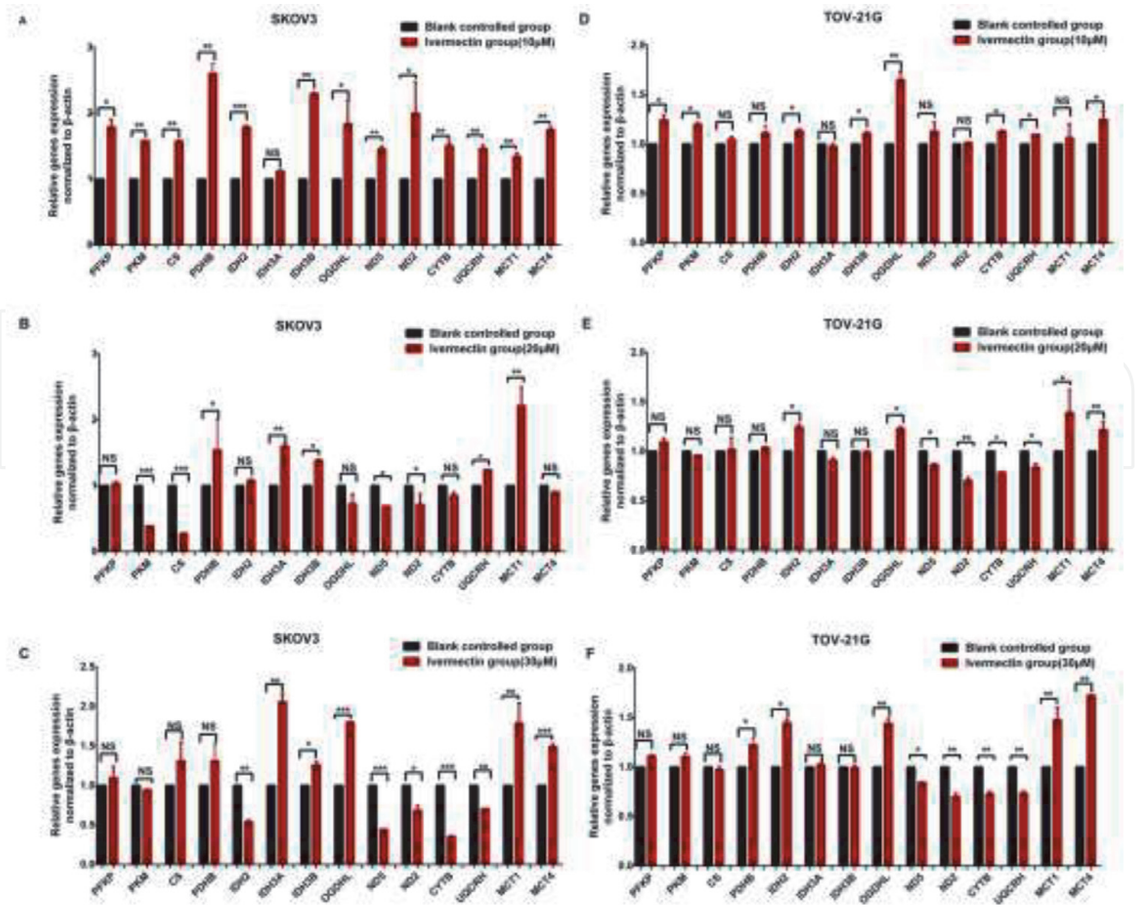

Figure 5.
*RT-qPCR confirmed the effects of ivermectin on the mRNA expressions of key molecules in the energy metabolism pathways in ovarian cancer cells (a-f). The effects of different concentration of ivermectin (0, 10, 20, and 30 μM) on mRNA expressions of PFKP, PKM, CS, PDHB, IDH2, IDH3A, IDH3B, OGDHL, ND5, ND2, CYTB, UQCRH, MCT1, and MCT4. n = 3. *p < 0.05, **p < 0.01, ***p < 0.001. Reproduced from Li et al. [21], with copyright permission from nature springer publisher, copyright 2020.*

with ovarian cancer survival rate. Among 306 EIF4A3-binding mRNAs, the protein expressions of 116 EIF4A3-binding mRNAs and EIF4A3 were found to be inhibited by ivermectin, identified by SILAC quantitative proteomics in ovarian cancer cells treated with and without ivermectin (**Table 2**) [4].

Moreover, TCGA transcriptomics analysis found that 16 lncRNAs had binding sites with EIF4A3 and associated with ovarian cancer survival rate, including SNHG3, HCG15, PDCD4-AS1, KIF9-AS1, ZNRF3-AS1, ZNF674-AS1, LINC00565, SOS1-IT1, WWTR1-AS1, PLCH1-AS1, LINC00517, STARD13-IT1, LEMD1-AS1, AL109767.1, HOXC-AS3, and LBX2-AS1 [23]. Further, RT-qPCR analysis of these 16 lncRNA expressions in ovarian cancer cells treated with ivermectin (0 μM, 10 μM, 20 μM, and 30 μM) compared to control cells, which found 9 lncRNAs (PDCD4-AS1, ZNRF3-AS1, HCG15, KIF9-AS1, LINC00565, ZNF674-AS1, AL109767.1, SOS1-IT1, and LBX2-AS1) were significantly affected by ivermectin (**Figure 7**) [4].

These findings clearly demonstrated that ivermectin regulated lncRNA-EIF4A3-mRNA axis in ovarian cancer cells, and these mRNAs included the key molecules in energy metabolism pathways in ovarian cancer cells.

3.8 The prognostic model of ivermectin-related three-lncRNA signature for ovarian cancers identified and optimized by lasso regression

Based on those nine ivermectin-mediated lncRNAs in ovarian cancers, survival analysis and lasso regression were used to identify and optimize the prognostic model of ivermectin-related three-lncRNA signature (ZNRF3-AS1,

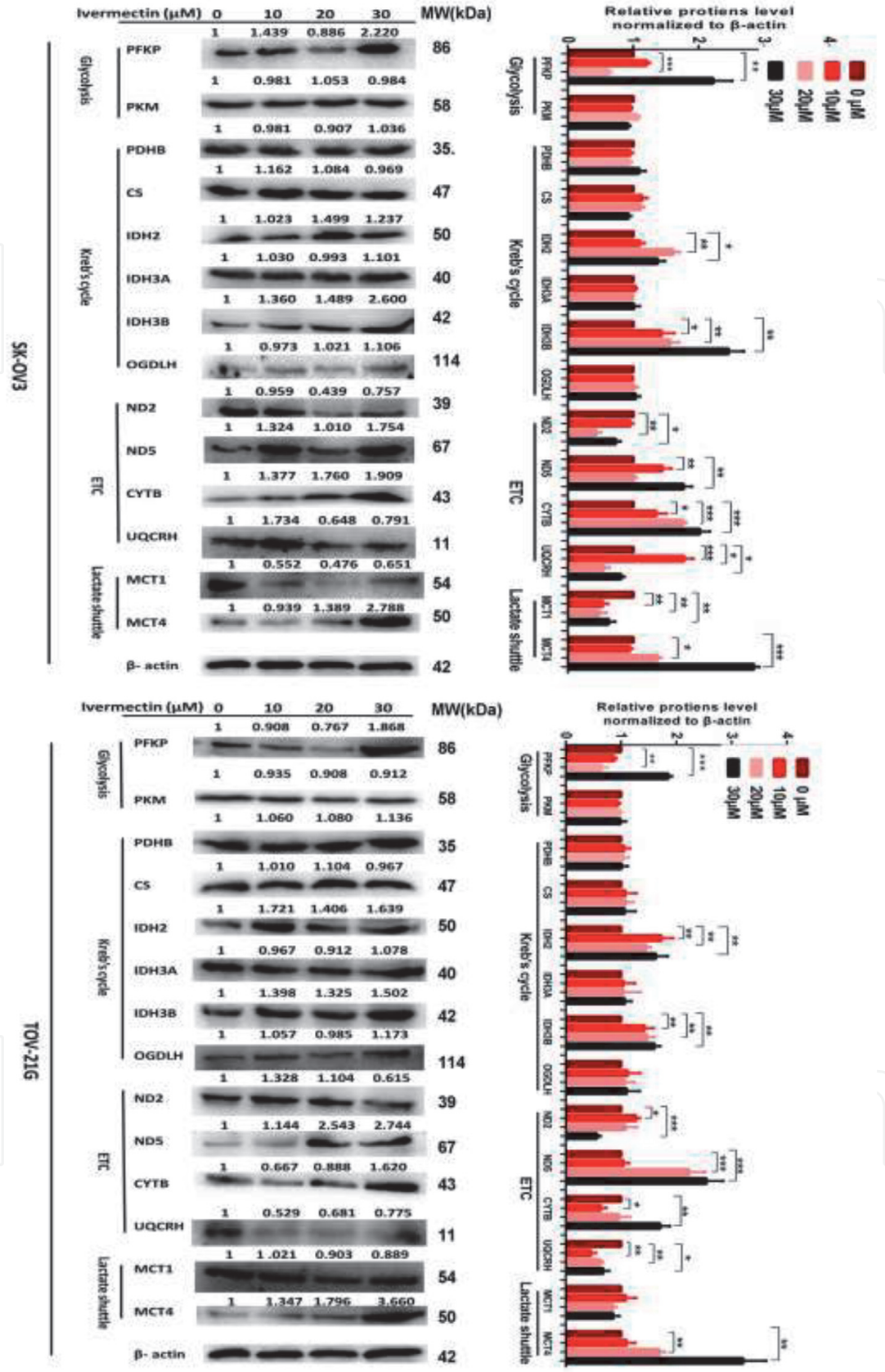

Figure 6.
*Western blot confirmed the effects of ivermectin on the protein expressions of key molecules in the energy metabolism pathways in ovarian cancer cells. n = 3. *p < 0.05, **p < 0.01, ***p < 0.001. Reproduced from Li et al. [21], with copyright permission from nature springer publisher, copyright 2020.*

SOS1-IT1, and LINC00565) (**Figure 8**) [4]. This prognostic model was significantly related to overall survival and clinicopathologic characteristics in ovarian cancer patients [4], which might benefit for prognostic assessment and personalized drug therapy toward 3P medicine practice in ovarian cancer.

Protein IDs	Protein names	Gene names	Q-value	Score	Intensity H	Intensity L	Ratio H/L
A0A0S2Z4C6	Serine/threonine-protein phosphatase 2B catalytic subunit alpha isoform	PPP3CA	0	106	450040000	2.321E+09	0.17
A0A024R7B0	Ubiquitin-like protein 5	UBL5	0	3	33400000	156360000	0.20
A0A024R9A9	Ubiquitin-conjugating enzyme E2 T	UBE2T	0	7	54580000	216150000	0.22
A0A494C101	Pyruvate carboxylase;Pyruvate carboxylase, mitochondrial	PC	0	3	3454600	19685000	0.28
A0A1W2PNM1	Hydroxyacyl-coenzyme A dehydrogenase, mitochondrial	HADH	0	11	85389000	332200000	0.30
Q496I0	Cytochrome c oxidase subunit 7A2, mitochondrial	COX7A2	0	10	223550000	687660000	0.32
Q149N6	Dedicator of cytokinesis protein 4	DOCK4	0	4	2402200	12153000	0.33
Q15036	Sorting nexin-17	SNX17	0	9	2545600	64295000	0.33
J3KN67	Tropomyosin alpha-3 chain	TPM3	0	3	44208000	225430000	0.34
Q8WZ82	Ovarian cancer-associated gene 2 protein	OVCA2	0	8	22175000	92294000	0.34
G3V0I5	NADH dehydrogenase [ubiquinone] flavoprotein 1, mitochondrial	NDUFV1	0	9	25550000	98424000	0.34
J3QLR8	28S ribosomal protein S23, mitochondrial	MRPS23	0	8	59957000	127510000	0.35
J3KSI8	28S ribosomal protein S7, mitochondrial	MRPS7	0	9	56198000	98108000	0.35
B4DP80	NAD(P)H-hydrate epimerase	APOA1BP	0	47	81014000	347980000	0.37
C9JFE4	COP9 signalosome complex subunit 1	GPS1	0	25	189930000	447320000	0.38
Q9Y3B7	39S ribosomal protein L11, mitochondrial	MRPL11	0	5	17279000	5213500	0.38
Q9Y333	U6 snRNA-associated Sm-like protein LSm2	LSM2	0	23	188570000	423780000	0.38
P63261	Actin	ACTG1	0	212	3.864E+09	1.674E+10	0.38
Q07954	Prolow-density lipoprotein receptor-related protein 1	LRP1	0	5	3971000	52428000	0.38
Q68E01	Integrator complex subunit 3	INTS3	0	11	32873000	113610000	0.38
K7EKI4	39S ribosomal protein L4, mitochondrial	MRPL4	0	9	41947000	121900000	0.39
V9GZ56	U6 snRNA-associated Sm-like protein LSm4	LSM4	0	4	89988000	217330000	0.39

Protein IDs	Protein names	Gene names	Q-value	Score	Intensity H	Intensity L	Ratio H/L
A0A0S2Z4T1	DNA replication licensing factor MCM3	MCM3	0	187	1.033E+09	3.186E+09	0.40
A0A0S2Z3L0	Electron transfer flavoprotein subunit alpha, mitochondrial	ETFA	0	44	623280000	1.382E+09	0.40
Q8NFH5	Nucleoporin NUP53	NUP35	0	81	206630000	398870000	0.40
Q5T7C4	High mobility group protein B1	HMGB1	0	98	2.916E+09	1.141E+10	0.40
A0A024R8M4	Phosphoribosyl pyrophosphate synthase-associated protein 1	PRPSAP1	0	20	88227000	200670000	0.41
G3V2D5	Zinc finger protein 36, C3H1 type-like 1	ZFP36L1	0	18	6238500	15019000	0.41
A6NMQ3	Alpha-endosulfine	ENSA	0	5	80231000	206330000	0.41
A0A0J9YYL3	Poly(U)-binding-splicing factor PUF60	PUF60	0	135	468910000	1.281E+09	0.42
A0A481SVJ4	Matrix-remodeling-associated protein 7	MXRA7	0	2	4184200	24167000	0.42
J3KTF8	Rho GDP-dissociation inhibitor 1	ARHGDIA	0	56	1.44E+09	3.59E+09	0.42
P49736	DNA replication licensing factor MCM2	MCM2	0	90	937140000	2.544E+09	0.43
K7EJH0	Kinetochore protein Spc24	SPC24	0	7	91278000	196000000	0.43
Q9BRA2	Thioredoxin domain-containing protein 17	TXNDC17	0	38	745240000	1.838E+09	0.43
P15531	Nucleoside diphosphate kinase A	NME1	0	20	312380000	966090000	0.43
D3DVA5	Rho guanine nucleotide exchange factor 2	ARHGEF2	0	16	26979000	80246000	0.44
B7ZM10	Exportin-6	XPO6	0	7	7924200	14822000	0.44
G8JLD3	ELKS/Rab6-interacting/CAST family member 1	ERC1	0	44	179630000	428430000	0.44
B2R7W3	Breast carcinoma amplified sequence 2	BCAS2	0	15	38190000	177190000	0.44
C9JJ19	28S ribosomal protein S34, mitochondrial	MRPS34	0	10	69862000	158490000	0.44
A0A0S2Z4Q4	Hepatocyte growth factor-regulated tyrosine kinase substrate	HGS	0	10	52165000	121060000	0.44
Q53Y51	D-dopachrome decarboxylase	DDT	0	36	259770000	672160000	0.45
A0A024R8U9	Pyrroline-5-carboxylate reductase 1, mitochondrial	PYCR1	0	20	72360000	265100000	0.45

Protein IDs	Protein names	Gene names	Q-value	Score	Intensity H	Intensity L	Ratio H/L
Q6FHQ0	Histone-binding protein RBBP7	RBBP7	0	160	2.134E+09	4.792E+09	0.45
P29144	Tripeptidyl-peptidase 2	TPP2	0	173	523060000	1.368E+09	0.45
Q9UP83	Conserved oligomeric Golgi complex subunit 5	COG5	0	5	14333000	32372000	0.46
E9PID8	Cleavage stimulation factor subunit 2	CSTF2	0	39	128240000	239460000	0.46
A0A024R496	Calcium-binding protein 39	CAB39	0	24	198430000	418650000	0.46
Q6IAP9	U4/U6 small nuclear ribonucleoprotein Prp4	PRPF4	0	42	168190000	621480000	0.46
A0A024RB32	Prostaglandin E synthase 3	PTGES3	0	110	2.02E+09	5.058E+09	0.46
E9PMG1	RalBP1-associated Eps domain-containing protein 1	REPS1	0	8	13894000	28102000	0.46
P28066	Proteasome subunit alpha type-5	PSMA5	0	107	1.677E+09	4.011E+09	0.46
I3L2G3	Ketosamine-3-kinase	FN3KRP	0	7	16246000	54477000	0.46
A0A0S2Z4Z0	RNA-binding protein 14	RBM14	0	83	606470000	1.446E+09	0.46
A8K651	Complement component 1 Q subcomponent-binding protein, mitochondrial	C1QBP	0	109	3.184E+09	7.587E+09	0.47
O60506	Heterogeneous nuclear ribonucleoprotein Q	SYNCRIP	0	121	3.657E+09	8.092E+09	0.47
P42345	Serine/threonine-protein kinase mTOR	MTOR	0	14	52206000	144780000	0.47
A8K878	Mesencephalic astrocyte-derived neurotrophic factor	MANF	0	38	604460000	1.613E+09	0.47
A0MNN4	Shwachman-Bodian-Diamond syndrome isoform 1	SMU1	0	60	321320000	679840000	0.47
A0A024R8B1	TBC1 domain family member 13	TBC1D13	0	4	20484000	74249000	0.47
Q9UHR4	Brain-specific angiogenesis inhibitor 1-associated protein 2-like protein 1	BAIAP2L1	0	6	21391000	41855000	0.47
Q5SRT3	Chloride intracellular channel protein 1	CLIC1	0	299	1.295E+10	2.924E+10	0.47
A0A0S2Z5I7	Ribosome maturation protein SBDS	SBDS	0	16	344540000	808860000	0.48
Q13505	Metaxin-1	MTX1	0	10	45737000	109770000	0.49
J3KS15	Peptidyl-tRNA hydrolase ICT1, mitochondrial	ICT1	0.01	2	29017000	45629000	0.50

Protein IDs	Protein names	Gene names	Q-value	Score	Intensity H	Intensity L	Ratio H/L
Q53HN4	DNA fragmentation factor subunit alpha	DFFA	0	31	272390000	539710000	0.50
P38919	Eukaryotic initiation factor 4A-III	EIF4A3	0	77	1.57E+09	3.534E+09	0.50
B4DY09	Interleukin enhancer-binding factor 2	ILF2	0	96	2.642E+09	6.06E+09	0.50
E9PF19	Transducin beta-like protein 2	TBL2	0	28	109400000	213970000	0.50
A0A087WXS7	ATPase ASNA1	ASNA1	0	63	850190000	1.755E+09	0.51
O43324	Eukaryotic translation elongation factor 1 epsilon-1	EEF1E1	0	29	662460000	1.236E+09	0.51
Q15717	ELAV-like protein 1	ELAVL1	0	92	2.093E+09	4.32E+09	0.51
Q9UMS4	Pre-mRNA-processing factor 19	PRPF19	0	127	897150000	2.364E+09	0.52
P14324	Farnesyl pyrophosphate synthase	FDPS	0	26	1.03E+09	2.078E+09	0.52
P28070	Proteasome subunit beta type-4	PSMB4	0	25	512090000	1E+09	0.52
Q0VGA5	SARS protein	SARS	0	149	1.216E+09	2.647E+09	0.53
A0A024RCX8	Peptidyl-prolyl cis-trans isomerase-like 1	PPIL1	0	10	122810000	365070000	0.53
Q9H8H0	Nucleolar protein 11	NOL11	0	5	22443000	80063000	0.54
E7EX90	Dynactin subunit 1	DCTN1	0	131	823150000	1.803E+09	0.54
Q05D78	Double-strand break repair protein MRE11A	MRE11A	0	3	24064000	56350000	0.54
H7C440	DIS3-like exonuclease 2	DIS3L2	0	4	13696000	21117000	0.54
Q9Y3U8	60S ribosomal protein L36	RPL36	0	34	544540000	770200000	0.55
Q9UJZ1	Stomatin-like protein 2, mitochondrial	STOML2	0	119	866230000	1.683E+09	0.55
Q567R6	Single-stranded DNA-binding protein, mitochondrial	SSBP1	0	60	561820000	1.077E+09	0.55
Q15084	Protein disulfide-isomerase A6	PDIA6	0	323	1.201E+10	2.023E+10	0.56
Q15645	Pachytene checkpoint protein 2 homolog	TRIP13	0	27	276670000	492930000	0.56
A0A024R6K8	Epididymis secretory sperm binding protein	WARS	0	80	1.769E+09	2.803E+09	0.56

Protein IDs	Protein names	Gene names	Q-value	Score	Intensity H	Intensity L	Ratio H/L
Q9NPD3	Exosome complex component RRP41	EXOSC4	0	25	239980000	490570000	0.57
Q9UHB9	Signal recognition particle subunit SRP68	SRP68	0	68	343910000	687640000	0.57
F5H0P4	Porphobilinogen deaminase	HMBS	0	9	38322000	129490000	0.57
Q96SB4	SRSF protein kinase 1	SRPK1	0	49	123510000	199050000	0.57
Q9Y6W5	Wiskott-Aldrich syndrome protein family member 2	WASF2	0	22	69082000	151250000	0.57
A0A024R8S5	Protein disulfide-isomerase	P4HB	0	300	1.656E+10	2.799E+10	0.57
A0A2X0SF71	Rho GTPase-activating protein 17	ARHGAP17	0	28	59467000	116590000	0.58
P09496	Clathrin light chain A	CLTA	0	7	508650000	765700000	0.58
R4GMU1	GDH/6PGL endoplasmic bifunctional protein	H6PD	0	4	20789000	34525000	0.60
Q8NCN5	Pyruvate dehydrogenase phosphatase regulatory subunit, mitochondrial	PDPR	0	3	10312000	28116000	0.60
Q8WY22	BRI3-binding protein	BRI3BP	0.01	2	5099700	6146700	0.62
Q6IB29	Probable rRNA-processing protein EBP2	EBNA1BP2	0	6	30468000	61825000	0.62
O15031	Plexin-B2	PLXNB2	0	18	30986000	221240000	0.62
C9JYQ9	60S ribosomal protein L22-like 1	RPL22L1	0	6	616860000	1.011E+09	0.66
Q9UNS2	COP9 signalosome complex subunit 3	COPS3	0	56	157900000	294180000	0.66
A0A0G2JNZ5	Glucosylceramidase	GBA	0	6	118570000	187510000	0.67
A0A140VK17	EH domain-binding protein 1	EHBP1	0	4	6547700	17018000	0.71
F5GWG3	Retinoic acid-induced protein 3	GPRC5A	0	11	149190000	185790000	0.76
S4R3V8	Lipolysis-stimulated lipoprotein receptor	LSR	0	4	26182000	34332000	1.05
Q9NWT6	Hypoxia-inducible factor 1-alpha inhibitor	HIF1AN	0	17	0	46940000	NaN
B7ZBQ1	Mediator of RNA polymerase II transcription subunit 20	MED20	0.01	2	0	18220000	NaN
H3BR38	Target of rapamycin complex subunit LST8	MLST8	0	3	0	13473000	NaN

Protein IDs	Protein names	Gene names	Q-value	Score	Intensity H	Intensity L	Ratio H/L
P52815	39S ribosomal protein L12, mitochondrial	MRPL12	0.01	2	0	0	NaN
A0A024R1I3	Pyridoxal phosphate phosphatase	PDXP	0	6	0	40714000	NaN
A0A2R8YDS2	Ras/Rap GTPase-activating protein SynGAP	SYNGAP1	0	2	0	18400000	NaN
J3KQA0	Synaptotagmin-1	SYT1	0	26	0	339450000	NaN
Q5W0C6	Torsin-3A	TOR3A	0	3	0	16493000	NaN
B4DSK7	Mediator of RNA polymerase II transcription subunit 1	MED1	0	2	0	14356000	NaN
Q99549	M-phase phosphoprotein 8	MPHOSPH8	0	12	0	15782000	NaN

Table 2.
The proteins of 116 EIF4A3-biding mRNAs and EIF4A3 were inhibited by ivermectin, identified with SILAC quantitative proteomics in ovarian cancer cells treated with (H) and without (L) ivermectin. Reproduced from Li et al. [4], with copyright permission from nature springer publisher, copyright 2020.

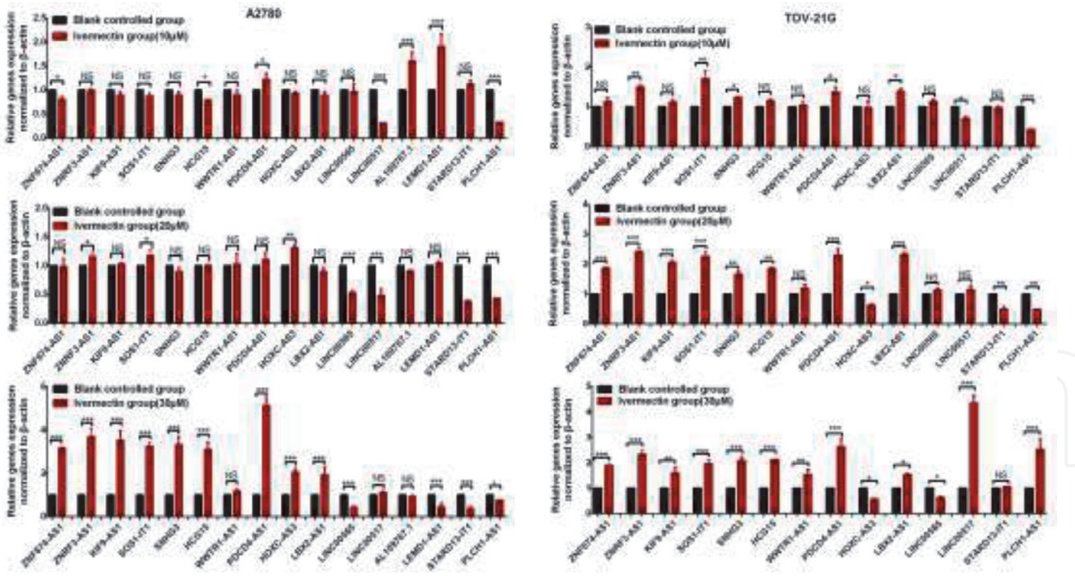

Figure 7.
RT-qPCR analysis revealed the effects of ivermectin on lncRNAs in ovarian cancers relative to control cells. Reproduced from Li et al. [4], with copyright permission from nature springer publisher, copyright 2020.

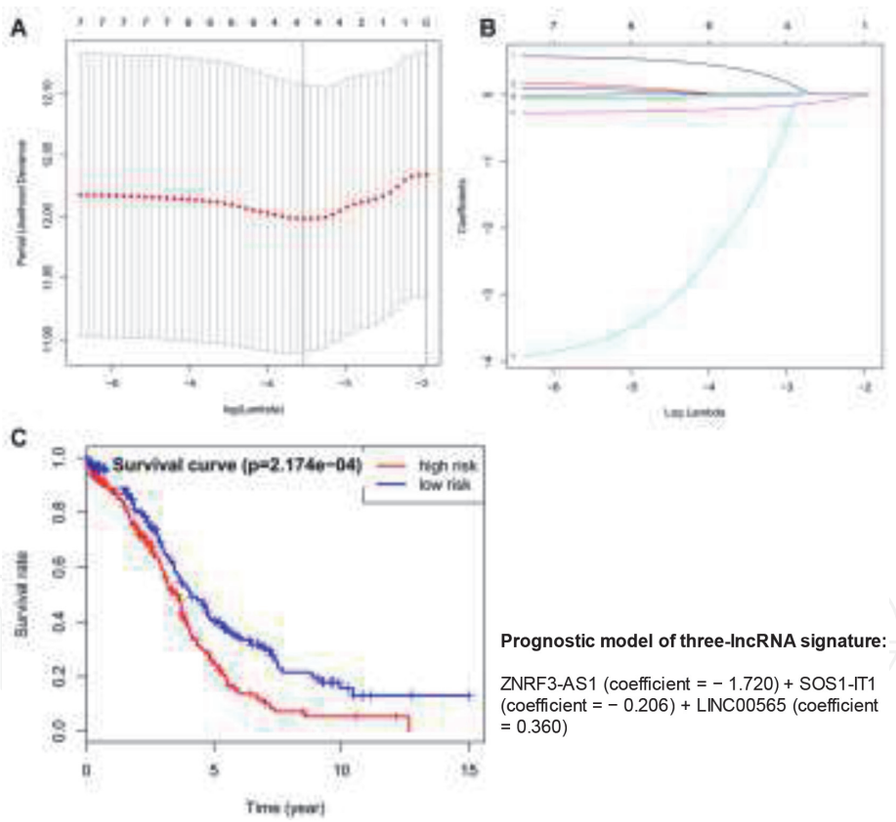

Figure 8.
Lasso regression identified and optimized the prognostic model of ivermectin-related three-lncRNA signature in ovarian cancers. (A and B). Lasso regression complexity is controlled by lambda using the glmnet R package. (C). Overall survival analysis of three-lncRNA signature between high-risk and low-risk groups. Reproduced from Li et al. [4], with copyright permission from nature springer publisher, copyright 2020.

4. Conclusions

Ivermectin, as an old, common, and classic anti-parasite drug, has demonstrated its effective *in vitro* anti-cancer efficiency for ovarian cancer. Ivermectin significantly inhibited cell proliferation, growth and migration, blocked cell cycle progression,

and promoted cell apoptosis of human ovarian cancer cells. Drug pathway network analysis of ivermectin revealed that it was significantly related to the key molecules of four energy metabolism pathways, and RT-qPCR and immunoaffinity blot analyses found that ivermectin significantly regulated these key molecules for those energy metabolism pathways, including PFKP in glycolysis, IDH2 and IDH3B in Kreb's cycle, ND2, ND5, CYTB, and UQCRH in oxidative phosphorylation, and MCT1 and MCT4 in lactate shuttle. The integrative analysis of TCGA transcriptomics and mitochondrial proteomics in ovarian cancer revealed that 16 survival-related lncRNAs were mediated by ivermectin, which were further confirmed with RT-qPRC in human ovarian cancer cells. SILAC quantitative proteomics analysis revealed that the expressions of RNA-binding protein EIF4A3 and 116 EIF4A3-interacted genes were extensively inhibited by ivermectin. Those 116 EIF4A3-interacted proteins included those key molecules in four energy metabolism pathways, and those lncRNAs regulated EIF4A3-mRNA axes. Thus, ivermectin mediated lncRNA-EIF4A3-mRNA axes in ovarian cancer to exert its anticancer activities. Moreover, lasso regression identified the prognostic model of ivermectin-related three-lncRNA signature (ZNRF3-AS1, SOS1-IT1, and LINC00565), which was significantly associated with overall survival and clinicopathologic characteristics of ovarian cancer patients. These ivermectin-related molecular pattern alterations benefit for prognostic assessment and personalized drug therapy in the context of 3P medicine practice in ovarian cancer.

Moreover, one must realize that these achieved data about the anti-cancer activities of ivermectin in ovarian cancers are derived from the *in vitro* cell models. It is necessary to expand it into the *in vivo* animal experiments and pre-clinical and clinical experiments for its real application in ovarian cancers.

Acknowledgements

The authors acknowledge the financial supports from the Shandong First Medical University Talent Introduction Funds (to X.Z.), the Hunan Provincial Hundred Talent Plan (to X.Z.), and the grants from China "863" Plan Project (Grant No. 2014AA020610-1 to XZ).

Conflict of interest

We declare that we have no financial and personal relationships with other people or organizations.

Author's contributions

X.Z. conceived the concept, designed the manuscript, wrote and critically revised the manuscript, coordinated and was responsible for the correspondence work and financial support. N.L. participated in preparing figures, and partial literature analysis.

Acronyms and abbreviations

FDA	Federal Drug Administration
mtDEPs	differentially mitochondrial proteins
RT-qPCR	quantitative real-time PCR
SILAC	stable isotope labeling with amino acids in cell culture
TCGA	The Cancer Genome Atlas

Author details

Xianquan Zhan[1,2*] and Na Li[1,2]

1 University Creative Research Initiatives Center, Shandong First Medical University, Jinan, Shandong, China

2 Key Laboratory of Cancer Proteomics of Chinese Ministry of Health, Xiangya Hospital, Central South University, Changsha, China

*Address all correspondence to: yjzhan2011@gmail.com

IntechOpen

References

[1] Burg RW, Miller BM, Baker EE, et al. Avermectins, new family of potent anthelmintic agents: producing organism and fermentation. Antimicrob Agents Chemother 1979; 15(3): 361–367.

[2] Crump A. Ivermectin: enigmatic multifaceted 'wonder' drug continues to surprise and exceed expectations. J Antibiot (Tokyo) 2017; 70(5): 495–505.

[3] Laing R, Gillan V, Devaney E. Ivermectin—old drug, new tricks? Trends Parasitol 2017; 33(6): 463–472.

[4] Li N, Zhan X. Anti-parasite drug ivermectin can suppress ovarian cancer by regulating lncRNA-EIF4A3-mRNA axes. EPMA J 2020; 11(2): 289–309.

[5] Li N, Zhao L, Zhan X. Quantitative proteomics reveals a broad-spectrum antiviral property of ivermectin, benefiting for COVID-19 treatment. J Cell Physiol 2020. DOI: 10.1002/jcp.30055.

[6] Liu J, Zhang K, Cheng L, Zhu H, Xu T. Progress in understanding the molecular mechanisms underlying the antitumour effects of ivermectin. Drug Des Devel Ther 2020; 14: 285–296.

[7] Juarez M, Schcolnik-Cabrera A, Duenas-Gonzalez A. The multitargeted drug ivermectin: from an antiparasitic agent to a repositioned cancer drug. Am J Cancer Res 2018; 8(2): 317–331.

[8] Kobayashi Y, Banno K, Kunitomi H, Tominaga E, Aoki D. Current state and outlook for drug repositioning anticipated in the field of ovarian cancer. J Gynecol Oncol 2019; 30(1): e10.

[9] Triarico S, Capozza MA, Mastrangelo S, Attinà G, Maurizi P, Ruggiero A. Gynecological cancer among adolescents and young adults (AYA). Ann Transl Med 2020; 8(6): 397.

[10] Li N, Zhan X. Mass spectrometry-based mitochondrial proteomics in human ovarian cancer. Mass Spectrom Rev 2020; 39(5–6): 471–498.

[11] Li N, Zhan X. Signaling pathway network alterations in human ovarian cancers identified with quantitative mitochondrial proteomics. EPMA J 2019; 10(2): 153–172.

[12] Li N, Li H, Cao L, Zhan X. Quantitative analysis of the mitochondrial proteome in human ovarian carcinomas. Endocr Relat Cancer 2018; 25(10): 909–931.

[13] Li N, Li J, Desiderio DM, Zhan X. SILAC quantitative proteomics analysis of vermectin-related proteomic profiling and molecular network alterations in human ovarian cancer cells. J Mass Spectrom 2020; e4659. DOI: 10.1002/jms.4659.

[14] Zhang X, Qin T, Zhu Z, et al. Ivermectin augments the in vitro and in vivo efficacy of cisplatin in epithelial ovarian cancer by suppressing Akt/mTOR signaling. Am J Med Sci 2020; 359(2): 123–129.

[15] Hashimoto H, Messerli SM, Sudo T, Maruta H. Ivermectin inactivates the kinase PAK1 and blocks the PAK1-dependent growth of human ovarian cancer and NF2 tumor cell lines. Drug Discov Ther 2009; 3(6): 243–246.

[16] Dou Q, Chen HN, Wang K, et al. Ivermectin induces cytostatic autophagy by blocking the PAK1/Akt axis in breast cancer. Cancer Res 2016; 76(15): 4457–4469.

[17] Song D, Liang H, Qu B, et al. Ivermectin inhibits the growth of glioma cells by inducing cell cycle arrest and apoptosis in vitro and in vivo. J Cell Biochem 2019; 120(1): 622–633.

[18] Nambara S, Masuda T, Nishio M, et al. Antitumor effects of the antiparasitic agent ivermectin via inhibition of Yes-associated protein 1 expression in gastric cancer. Oncotarget 2017; 8(64): 107666–107677.

[19] Melotti A, Mas C, Kuciak M, Lorente-Trigos A, Borges I, Ruiz i Altaba A. The river blindness drug ivermectin and related macrocyclic lactones inhibit WNT-TCF pathway responses in human cancer. EMBO Mol Med 2014; 6(10): 1263–1278.

[20] Slade L, Pulinilkunnil T. The MiTF/TFE family of transcription tactors: master regulators of organelle signaling, metabolism, and stress adaptation. Mol Cancer Res 2017; 15(12):1637–1643.

[21] Li N, Li H, Wang Y, Cao L, Zhan X. Quantitative proteomics revealed energy metabolism pathway alterations in human epithelial ovarian carcinoma and their regulation by the antiparasite drug ivermectin: data interpretation in the context of 3P medicine. EPMA J 2020; 11: 661–694.

[22] Guzzo CA, Furtek CI, Porras AG, Chen C, Tipping R, Clineschmidt CM, Lasseter KC. Safety, tolerability, and pharmacokinetics of escalating high doses of ivermectin in healthy adult subjects. J Clin Pharmacol. 2002; 42(10): 1122–1133.

[23] Li N, Zhan X, Zhan X. The lncRNA SNHG3 regulates energy metabolism of ovarian cancer by an analysis of mitochondrial proteomes. Gynecol Oncol. 2018; 150: 343–354.